JOC Article

Dynamic Proton-Induced Emission Switching in Donor-Functionalized Dehydrobenzopyrid[15]annulenes

Eric L. Spitler, Sean P. McClintock, and Michael M. Haley*

Department of Chemistry and Materials Science Institute, University of Oregon, Eugene, Oregon 97403-1253

haley@uoregon.edu

Received April 19, 2007

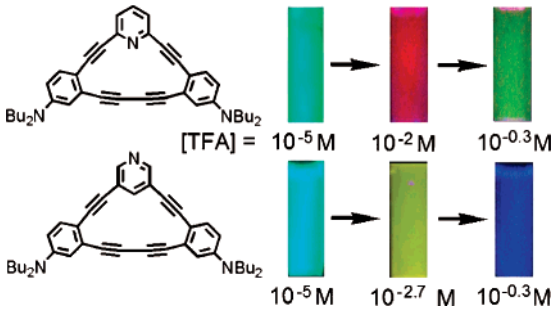

An isomeric pair of 15-membered dehydrobenzopyridannulenes functionalized with $-NBu_2$ groups as π-electron donors was prepared and their steady-state spectroscopic parameters investigated. The property differences arising from placement of the pyridine nitrogen relative to the macrocycle, as well as the differential effects of stepwise protonation of the acceptor and donor nitrogens, were examined. The macrocycles exhibited dynamic shifting in the emission spectra, which is believed to correlate to induced changes in the frontier molecular orbitals of the molecules.

Introduction

Highly conjugated, carbon-rich organic molecules have been the focus of extensive interest in recent years because of their unique optical and electronic properties.[1−3] In particular, chromophoric or fluorophoric systems possessing electronic and/or photonic transfer pathways are recognized as ideal candidates for components of analytical reagents and advanced optical devices.[4−8] Their propensity to act as bulk materials or organic liquid crystal arrays also implies applications in OLED, organic semiconductor, and photoelectric cell design.

We have been investigating the optoelectronic properties of a special class of carbon-rich compounds, dehydrobenzoannulenes (DBAs, Figure 1a).[4a−c] These fully conjugated macrocycles composed of acetylene-linked arenes represent attractive targets

* Address correspondence to this author. Fax: 541-346-0487. Phone: 541-346-0456.

(1) (a) de Meijere, A., Ed. *Topics in Current Chemistry* (*Carbon Rich Compounds I*); Springer: Berlin, Germany, 1998; Vol. 196. (b) de Meijere, A., Ed. *Topics in Current Chemistry (Carbon Rich Compounds II)*; Springer: Berlin, Germany, 1999; Vol. 201. (c) Diederich, F.; Stang, P. J.; Tykwinski, R. R., Eds. *Acetylene Chemistry*: *Chemistry, Biology, and Material Science*; Wiley-VCH: Weinheim, Germany, 2005. (d) Haley, M. M.; Tykwinski, R. R., Eds. *Carbon-Rich Compounds*: *From Molecules to Materials*; Wiley-VCH: Weinheim, Germany, 2006.

(2) Reviews, inter alia: (a) *Organic Light Emitting Devices*: *Synthesis, Properties and Applications*; Müllen, K., Scherf, U., Eds.; Wiley-VCH: Weinheim, Germany, 2006. (b) Chen, J.; Reed, M. A.; Dirk, S. M.; Price, D. W.; Rawlett, A. M.; Tour, J. M.; Grubisha, D. S.; Bennett, D. W. In *NATO Science Series II*: *Mathematics, Physics, Chemistry* (*Molecular Electronics*: *Bio-Sensors and Bio-Computers*); Plenum: New York, 2003; Vol. 96, pp 59−195. (c) Domerco, B.; Hreha, R. D.; Zhang, Y.-D.; Haldi, A.; Barlow, S.; Marder, S. R.; Kippelen, B. *J. Polym. Sci. Part B*: *Polym. Phys.* **2003**, *41*, 2726−2732. (d) Shirota, Y. *J. Mater. Chem.* **2000**, *10*, 1−25. (e) Schwab, P. F. H.; Levin, M. D.; Michl, J. *Chem. Rev.* **1999**, *99*, 1863−1933. (f) *Electronic Materials*: *The Oligomer Approach*; Müllen, K., Wegner, G., Eds.; Wiley-VCH: Weinheim, Germany, 1998. (g) *Nonlinear Optics of Organic Molecules and Polymers*; Nalwa, H. S., Miyata, S., Eds.; CRC Press: Boca Raton, FL, 1997.

(3) Recent examples, inter alia: (a) Kang, H.; Evrenenko, G.; Dutta, P.; Clays, K.; Song, K.; Marks, T. J. *J. Am. Chem. Soc.* **2006**, *128*, 6194−6205. (b) Knox, J. E.; Halls, M. D.; Hratchian, H. P.; Schlegel, H. B. *Phys. Chem. Chem. Phys.* **2006**, *8*, 1371−1377. (c) Shukla, V. K.; Kumar, S.; Deva, D. *Synth. Met.* **2006**, *156*, 387−391. (d) Seminario, J. M. *Nature Mater.* **2005**, *4*, 111−113. (e) Hughes, G.; Bryce, M. R. *J. Mater. Chem.* **2005**, *15*, 94−107. (f) Van der Auweraer, M.; De Schryver, F. C. *Nature Mater.* **2004**, *3*, 507−508. (g) Special Issue on Organic Electronics. *Chem. Mater.* **2004**, *16*, 4381−4846. (h) Simpson, C. D.; Wu, J.; Watson, M. D.; Müllen, K. *J. Mater. Chem.* **2004**, *14*, 494−504.

(4) (a) Marsden, J. A.; Miller, J. J.; Shirtcliff, L. D.; Haley, M. M. *J. Am. Chem. Soc.* **2005**, *127*, 2464−2476. See also: (b) Marsden, J. A.; Haley, M. M. *Angew. Chem., Int. Ed.* **2004**, *43*, 1694−1697. (c) Miller, J. J.; Marsden, J. A.; Haley, M. M. *Synlett* **2004**, 165−168. (d) Spitler, E. L.; Shirtcliff, L. D.; Haley, M. M. *J. Org. Chem.* **2007**, *72*, 86−96. (e) Samori, S.; Tojo, S.; Fujitsuka, M.; Spitler, E. L.; Haley, M. M.; Majima, T. *J. Org. Chem.* **2007**, *72*, 2785−2793.

10.1021/jo070827c CCC: $37.00 © 2007 American Chemical Society
Published on Web 08/09/2007

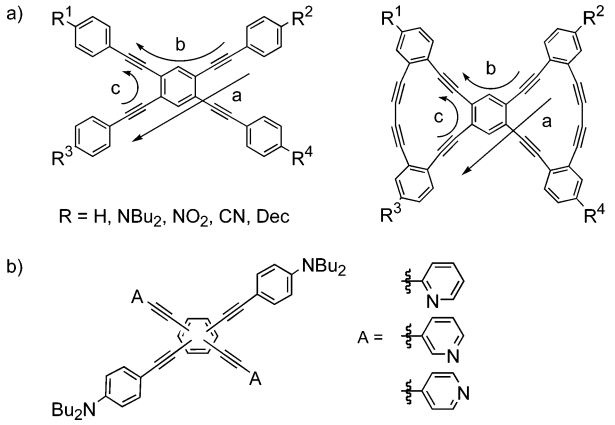

FIGURE 1. (a) Conjugated pathways present in structurally related tetrakis(phenylethynyl)benzenes and bis(dehydrobenzoannuleno)benzenes and (b) donor/acceptor tetrakis(arylethynyl)benzenes with dibutylaniline donors and pyridine acceptors.

of fundamental study into aromaticity and enforced planarization. We have also performed studies on donor/acceptor-functionalized DBAs that undergo intramolecular charge transfer upon optical excitation, as well as studies of their acyclic tetrakis(arylethynyl)benzene analogues (TAEBs) with variation of the acceptor group. Most recently, we reported a systematic study of isomeric pyridine-derivatized bisdonor/bisacceptor TAEBs (Figure 1b).[4d] We demonstrated that these systems underwent two-stage fluorescence emission shifting (to varying extents corresponding to charge-transfer pathway efficiency) upon titration with acid or addition of assorted metal ions, and

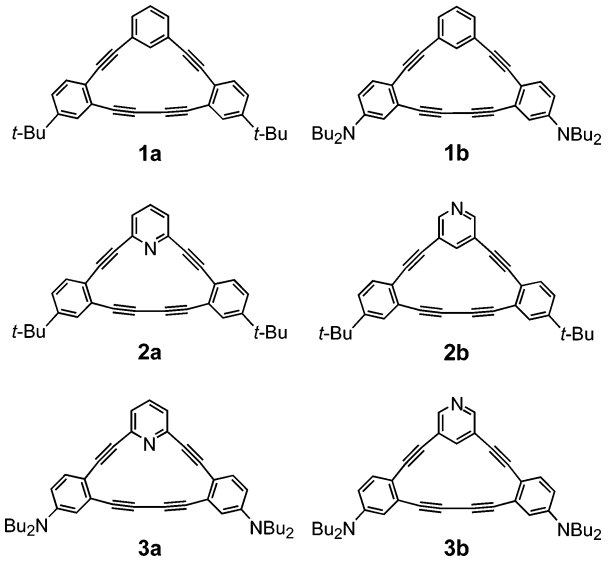

FIGURE 2. Fifteen-membered carbon macrocycle DBAs (**1**), *tert*-butyl functionalized DBPAs (**2**), and target donor-functionalized DBPAs (**3**).

that these shifts correlated to the relative energies of the spatially separate frontier molecular orbitals (FMOs). Thus, the segment-localized FMOs in conjugated donor/acceptor fluorophores could be manipulated independently.[9]

We have previously examined DBAs of the type **1**, incorporating solublizing *t*-Bu groups or electron-donating NBu_2 groups, as well as isomers of *t*-Bu-functionalized dehydrobenzopyridannulenes (DBPAs) **2**, fused at either the 2,6- or 3,5-positions (Figure 2).[10a−c] Tobe et al. have also prepared [15]DBAs in the course of examining more complex cyclophane architectures,[10d] and Baxter et al. have synthesized several related pyridannulene structures.[5e] We now present donor-functionalized DBPAs of the type **3**, which incorporate the aforementioned switching behavior into 15-membered acetylenic macrocycles. As moderate strength acceptors, pyridines can participate in various degrees of intramolecular charge transfer, depending on the efficiency of the conjugated pathway from the donor to the acceptor nitrogen.[4d] Since both donor and acceptor group(s) can be protonated, the ability to probe independent manipulation of the FMOs using shifts in the emission spectra can also be demonstrated.

Results and Discussion

Synthesis. Assembly of **3a** and **3b** is readily accomplished as shown in Scheme 1. Donor-functionalized alkyne segment **4**[4a] is appended to either 2,6- or 3,5-dibromopyridine **5** by using methanolic KOH to remove the more labile trimethylsilyl (TMS)

(5) (a) Bunz, U. H. F.; Rubin, Y.; Tobe, Y. *Chem. Soc. Rev.* **1999**, 107−119. (b) Haley, M. M.; Wan, W. B. In *Advances in Strained and Interesting Organic Molecules*; Halton, B., Ed.; JAI Press: Greenwich, CT, 2000; Vol. 8, pp 1−41. (c) Watson, M. D.; Fechtenkötter, A.; Müllen, K. *Chem. Rev.* **2001**, *101*, 1267−1300. (d) Nielsen, M. B.; Diederich, F. In *Modern Arene Chemistry;* Astruc, D., Ed.; Wiley-VCH: Weinheim, Germany, 2002; pp 196−216. (e) Baxter, P. N. W.; Dali-Youcef, R. *J. Org. Chem.* **2005**, *70*, 4935−4953.

(6) Inter alia: (a) Zhao, Y.; Slepkov, A. D.; Akoto, C. O.; McDonald, R.; Hegmann, F. A.; Tykwinski, R. R. *Chem. Eur. J.* **2005**, *11*, 321−329. (b) Bunz, U. H. F. *Adv. Polym. Sci.* **2005**, *177*, 1−52. (c) Fasina, T. M.; Collings, J. C.; Lydon, D. P.; Albesa-Jove, D.; Batsanov, A. S.; Howard, J. A. K.; Nguyen, P.; Bruce, M.; Scott, A. J.; Clegg, W.; Watt, S. W.; Viney, C.; Marder, T. B. *J. Mater. Chem.* **2004**, *14*, 2395−2404. (d) Boydston, A. J.; Yin, Y.; Pagenkopf, B. L. *J. Am. Chem. Soc.* **2004**, *126*, 3724−3725. (e) Gonzalo-Rodriguez, J.; Esquivias, J.; Lafuente, A.; Diaz, C. *J. Org. Chem.* **2003**, *68*, 8120−8128. (f) Bunz, U. H. F. *Chem. Rev.* **2000**, *100*, 1605−1644. (g) Tykwinski, R. R.; Gubler, U.; Martin, R. E.; Diederich, F.; Bosshard, C.; Günter, P. *J. Phys. Chem. B* **1998**, *102*, 4451−4465. (h) Tykwinski, R. R.; Schreiber, M.; Carlón, R. P.; Diederich, F.; Gramlich, V. *Helv. Chim. Acta* **1996**, *79*, 2249−2280. (i) Tahara, K.; Furukawa, S.; Uji-i, H.; Uchino, T.; Ichikawa, T.; Zhang, J.; Mamdouh, W.; Sonoda, M.; De Schryver, F. C.; De Feyter, S.; Tobe, Y. *J. Am. Chem. Soc.* **2006**, *128*, 16613−16625.

(7) (a) Slepkov, A.; Marsden, J. A.; Miller, J. J.; Shirtcliff, L. D.; Haley, M. M.; Kamada, K.; Tykwinski, R. R.; Hegmann, F. A. Nonlinear Optical Transmission and Multiphoton Processes in Organics III. *Proc. SPIE* **2005**, *5934*, 29−34. (b) Zhang, X.-B.; Feng, J.-K.; Ren, A.-M.; Sun, C.-C. *Opt. Mater.* **2007**, *29*, 955−962. (c) Slepkov, A.; Hegmann, F. A.; Tykwinski, R. R.; Kamada, K.; Ohta, K.; Marsden, J. A.; Spitler, E. L.; Miller, J. J.; Haley, M. M. *Opt. Lett.* **2006**, *31*, 3315−3317.

(8) (a) Bazan, G. C.; Bartholomew, G. P. *J. Am. Chem. Soc.* **2002**, *124*, 5183−5196. (b) Bazan, G. C.; Bartholomew, G. P. *Synthesis* **2002**, 1245−1255. (c) Nguyen, P.; Lesley, G.; Marder, T. B. *Chem. Mater.* **1997**, *9*, 406−408. (d) Meier, H.; Mühling, B.; Kolshorn, H. *Eur. J. Org. Chem.* **2004**, 1033−1042. (e) Meier, H.; Gerold, J.; Kolshorn, H.; Mühling, B. *Chem. Eur. J.* **2004**, *10*, 360−370. (f) Zimmerman, B.; Baranovic, G.; Stefanic, Z.; Rozman, M. *J. Mol. Struct.* **2006**, *794*, 115−124. (g) Wakabayashi, S.; Kato, Y.; Mochizuki, K.; Suzuki, R.; Matsumoto, M.; Sugihara, Y.; Shimizu, M. *J. Org. Chem.* **2007**, *72*, 744−749.

(9) (a) Wilson, J. N.; Bunz, U. H. F. *J. Am. Chem. Soc.* **2005**, *127*, 4124−4125. (b) Zucchero, A. J.; Wilson, J. N.; Bunz, U. H. F. *J. Am. Chem. Soc.* **2006**, *128*, 11872−11881. (c) Wilson, J. N.; Josowicz, M.; Wang, Y. Q.; Bunz, U. H. F. *Chem. Commun.* **2003**, 2962−2963.

(10) (a) Johnson, C. A.; Haley, M. M.; Rather, E.; Han, F.; Weakley, T. J. R. *Organometallics* **2005**, *24*, 1161−1172. (b) Johnson, C. A.; Baker, B. A.; Berryman, O. B.; Zakharov, L. N.; O'Connor, M. J.; Haley, M. M. *J. Organomet. Chem.* **2006**, *691*, 413−421. (c) Marsden, J. A.; Miller, J. J.; Haley, M. M. *Angew. Chem., Int. Ed.* **2004**, *43*, 1694−1697. (d) Tobe, Y.; Kishi, J.; Ohki, I.; Sonoda, M. *J. Org. Chem.* **2003**, *68*, 3330−3332.

(11) Calculated from the steady-state spectra with the techniques described in: Drushel, H. V.; Sommers, A. L.; Cox, R. C. *Anal. Chem.* **1963**, *35*, 2166−2172.

SCHEME 1. Preparation of DBPAS 3a and 3b

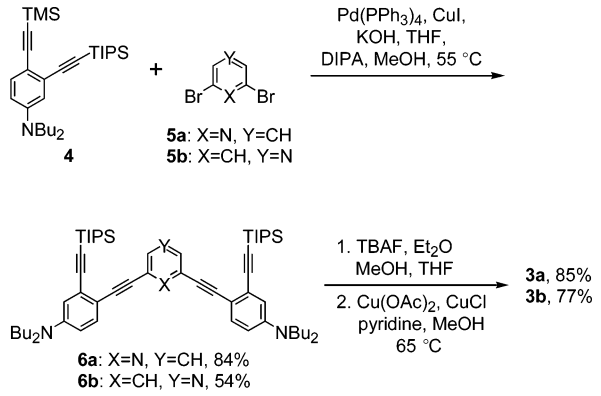

group in situ to afford the bisdonor precursors **6a** and **6b**. Removal of the triisopropylsilyl (TIPS) groups with tetrabutylammonium fluoride (TBAF) followed by oxidative intramolecular homocoupling under Cu-mediated conditions furnished macrocycles **3a** and **3b** in 71% and 42% overall yield, respectively. It is notable that in both coupling steps, the more conjugated systems **a** proceed in somewhat higher yields, a trend also observed in preparation of **2a** and **2b**.[10b]

In the strong donor/strong acceptor bisannulenes,[4a] significant self-associative behavior was observed in their ^{1}H NMR spectra due to intermolecular π-stacking and dipole attraction between respective donor and acceptor groups. In **3a** and **3b**, no such behavior was observed: NMR signals remained constant over a several-fold concentration gradient. There were, however, noticeable upfield shifts of the signals from protons ortho to the monoacetylene linkages ($\Delta\delta = 0.1-0.3$ ppm) upon ring closure of **6a**,**b** to **3a**,**b**, with smaller upfield shifts in other signals (see the Experimental Section and the Supporting Information). This effect is indicative of increased electron delocalization along the π-conjugated pathway. Upon cyclization to **3b**, there was a dramatic (0.91 ppm) downfield shift of the proton internal to the macrocycle, which was also observed in **2b**,[10b] and is attributed to the anisotropy of the nearby triple bonds.

Crystals of **3a** and **3b** suitable for X-ray diffraction were obtained by evaporation from 5:1:1 and 5:3:1 solutions of hexanes:CH_2Cl_2:EtOAc, respectively. Both DBPAs are planar structures with remarkably linear diyne bridges ($C_{sp}-C_{sp}$ bond angles for **3a** 177−179°and for **3b** 177−178°; Figures S4a and S5a in the Supporting Information). Most of the strain in the molecules is contained in the monoacetylene units, which are moderately distorted ($C_{sp}-C_{sp}$ bond angles for **3a** 167−174° and for **3b** 163−171°). Overall, the structures closely resemble the purely hydrocarbon [15]DBA reported by Tobe et al.[10d] In the solid state, **3b** packs in slipped π-stacking arrangement, similar to Tobe's annulene, whereas **3a** contains two symmetrically independent molecules arranged in zigzagging dimeric pairs. The packing differences are likely due to weak hydrogen bonding in **3b** between the pyridine nitrogen atom and an ortho pyridine proton on a neighboring molecule (N••·H−C distance 2.62 Å, Figure S5b, Supporting Information).

Absorption and Emission Data. Electronic absorption and emission spectra of **3a**,**b** are shown in Figure 3a and summarized in Table 1, along with their respective precursors **6a**,**b** and *tert*-butyl-functionalized analogues **2a**,**b**[10b] for comparison. Cyclization/planarization to the macrocycle enhances π-orbital overlap, increasing the conjugation. This results in a 17−25 nm bathochromic shift in the absorption spectra of **3a**,**b** versus **6a**,**b**, accompanied by a significant loss of intensity of the lowest energy band, possibly indicating weak intramolecular charge transfer. This is in good agreement with our previously described donor/acceptor bisannulene series, as well as recent examples of weak donor/weak acceptor-functionalized DBAs.[8f] The electron density from the donating groups results in a λ_{max} of the lowest energy bands in **3a** and **3b** that are 7 and 19 nm greater than those for **2a** and **2b**, respectively. It is somewhat surprising that the charge-transfer bands for **3a** and **3b** are so similar, since **3b** does not contain a direct resonance pathway for full conjugation, implying good inductive withdrawal by the pyridine ring as a unit.

Normalized emission spectra are shown in Figure 3b and Table 1. There is a dramatic red shift in both systems upon planarization. FMO plots (see next section) show significant LUMO density localized on the diacetylene bridges, so it is possible that cyclization has a more pronounced effect on the excited state energies, thus affecting the emission spectra more than the absorption. In the precursors, the more conjugated 2,6-fused system **6a** is more red-shifted, but in the annulenes the λ_{max} values are very similar. This may be due to the larger predicted net dipole in **3b** (8.46 D vs 4.25 D for **3a**, see Table S1 in the Supporting Information). The large increase in Stokes shifts upon ring closure also indicates an increase in net dipole and the efficiency of the conjugated π-system.[12] Our previous DBA studies generally show a *decrease* in Stokes shift upon planarization, but in some π-electron-rich species an increase is seen when there is significant calculated LUMO density on the bridging pathway.[4a] This also seems to be the case for the weak donor/acceptor systems here, and is likely due to the less effective cross-conjugated pathways present in the 15-membered macrocycles. Donor functionalization also results in maxima significantly red-shifted relative to **2a**,**b**,[10b] in agreement with previous DBA behavior.[4a]

There is little difference in Φ_f between **3a** and **3b**, likely reflecting the weak intramolecular charge-transfer transitions dominating in both. This agrees with previous results wherein the all-donor analogues of the systems in Figure 1 show higher quantum yields than the donor/acceptor systems.[4,13] Interestingly, the values for **3a** and **3b** are comparable to those for **2a** and **2b**. One would expect functionaliztion with donor π-electrons to increase Φ_f. The emission spectra of **2a** and **2b** contain significant fine structure, however, perhaps implying more complex vibronic interactions than are observed here. Cycles **2a** and **2b** also possess exceptionally long absorption cutoffs.[10b] The remarkably high quantum yields of precursors **6a** and **6b** help illustrate in part the effect of enforced planarization on the conjugation, but it is likely that the increased fluorescence is also due in part to donor electron contribution from the TIPS groups. Examination of desilylated **6a**,**b**, however, showed no significant effect on either absorption or emission wavelengths (see Figure S1 in the Supporting Information).

Molecular Orbital Plots. In our previously described ethynylpyridine systems,[4d] the ability to protonate the donor and acceptor segments independently resulted in a two-stage emis-

(12) (a) Anstead, G. M.; Katzenellenbogen, J. A. *J. Phys. Chem.* **1988**, *92*, 6249−6258. (b) Lackowicz, J. R. *Principles of Fluorescence Spectroscopy*; Plenum: New York, 1983.

(13) (a) Tolbert, L. M.; Nesselroth, S. M.; Netzel, T. L.; Raya, N.; Stapleton, M. *J. Phys. Chem.* **1992**, *96*, 4492−4496. (b) Englman, R.; Jortner, *J. Mol. Phys.* **1970**, *18*, 145−154. (c) Caspar, J. V.; Meyer, T. J. *J. Phys. Chem.* **1983**, *87*, 952−957.

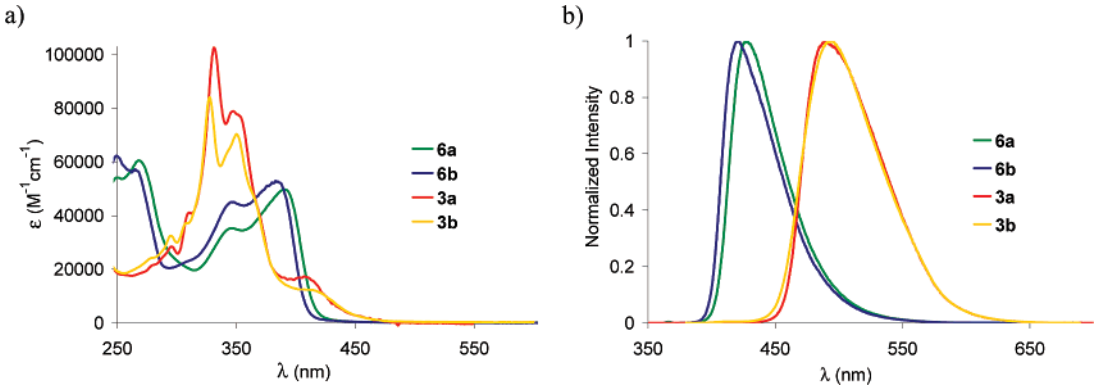

FIGURE 3. (a) Absorption and (b) emission spectra of DBPAs **3a**,**b** and precursors **6a**,**b** in CH_2Cl_2 at 20−30 μM concentration. Excitation at 365 nm.

TABLE 1. Electronic Absorption and Emission Data for 2a,b, 3a,b, and 6a,b

compd	lowest energy abs λ_{max} [nm] (ϵ [M^{-1} cm^{-1}])	em λ_{max} [nm]	Stokes shift [cm^{-1} (nm)]	Φ_f [c]
2a	400 (sh) (1750)[a]	454[b]	2974 (54)	0.16
2b	389 (3000)[a]	436[b]	2771 (47)	0.20
6a	390 (49760)	427	2222 (37)	0.81
6b	383 (52910)	421	2357 (38)	0.85
3a	407 (17290)	490	4162 (83)	0.19
3b	~408 (sh) (12410)	494	~4267 (86)	0.17

[a] Reference 10b. [b] Maxima corrected from ref 10b due to instrument error. [c] Calculated relative to fluorescein at pH 8 (ref 11) with excitation at lowest energy abs λ_{max}.

sion switching behavior, analogous to that first observed by Bunz and co-workers in related donor/acceptor cruciforms.[9a,b] Initial protonation with trifluoroacetic acid (TFA) caused a dramatic blue shift in the spectra, followed by a more modest red shift with subsequent protonation. Since the HOMO and LUMO are calculated to be localized primarily on the donor and acceptor segments, respectively, protonation of the donor or acceptor nitrogens causes the shifts by affecting the relative energies of the orbitals. Molecules **3a** and **3b** are similar systems, but with enforced planarization and with only one acceptor unit for two donor units.

FMO plots of **3a′** and **3b′** were calculated by using Gaussian03[14] (B3LYP[15] level of theory, 6-31G* basis set) with simplified structures that replaced the NBu_2 donor with NMe_2 (Figure 4). They predict largely overlapping HOMO and LUMO localizations in the neutral state, but protonation of the pyridine nitrogen and subsequent protonation of a donor nitrogen cause increasing spatial separation of the orbitals. Protonation of **3a′** to **3a′**$^+$ leaves the HOMO relatively unchanged and results in weak localization in the LUMO at the pyridine ring, but overall has little affect. Further protonation at one of the donor sites reveals a more separate orbital diagram in which the HOMO is localized largely on the neutral donor while the LUMO is spread over the protonated regions of the macrocycle, creating a more charge transfer-like system (although the FMOs are more separated in these cases, it is possible that both donor segments are in fact protonated in a dynamic equilibrium that does not lead to the orbital diagrams shown). Charge transfer is quenched by protonation of the final donor segment, causing overlapping molecular orbitals. Examination of **3b′** indicates that upon protonation the system exhibits more orbital localization than **3a′**, presumably due to the lack of a conjugated pathway. Protonation of the acceptor segment localizes the HOMO onto the two donor segments and the LUMO on the acceptor. Subsequent protonation of a donor segment results in localization of the HOMO around the neutral donor arene, while the LUMO is spread out between the two protonated segments. Both systems indicate that while the molecular orbitals are not fully separate, stepwise protonation of the systems may allow for manipulation of the orbitals and potentially their emission properties. The band gap energies for **3a′** and **3b′** were also calculated and found to be within 25 nm of the experimental band gaps for **3a** and **3b**, which is closer than calculated for previously examined DBAs (see Table S1 in the Supporting Information).[4a] Thus, stepwise protonation in **3a** and/or **3b** reflects an *induced* strong donor/acceptor species, implying enhanced charge-transfer character more akin to that predicted and observed in the ethynylpyridine systems, and therefore similar emission switching behavior for **3a**,**b**.

TFA Titrations. Trifluoroacetic acid (TFA) titration of **3a** in MeOH between [TFA] = 10^{-5} and $10^{-0.3}$ M showed no such switching behavior, and resulted only in qualitative quenching of fluorescent intensity with no change in wavelength (see Figure S2 in the Supporting Information). Repeating the titration of **3a** with TFA in CH_2Cl_2, on the other hand, yielded far different results (Figure 5). At [TFA] = 10^{-3} M, the original charge-transfer band at 407 nm in the absorption spectrum is greatly enhanced, and two new bands at 494 and 619 nm appear. These bands reach maximum intensity at [TFA] = 10^{-2} M, at which the solution attains a pale green color in ambient light. In the emission spectra, a rapid drop-off of fluorescent intensity is accompanied by the simultaneous appearance of a low-intensity peak at ca. 670 nm, shifting from bright blue-green fluorescence

(14) Frisch, M. J.; Trucks, G. W.; Schlegel, H. B.; Scuseria, G. E.; Robb, M. A.; Cheeseman, J. R.; Montgomery, J. A., Jr.; Vreven, T.; Kudin, K. N.; Burant, J. C.; Millam, J. M.; Iyengar, S. S.; Tomasi, J.; Barone, V.; Mennucci, B.; Cossi, M.; Scalmani, G.; Rega, N.; Petersson, G. A.; Nakatsuji, H.; Hada, M.; Ehara, M.; Toyota, K.; Fukuda, R.; Hasegawa, J.; Ishida, M.; Nakajima, T.; Honda, Y.; Kitao, O.; Nakai, H.; Klene, M.; Li, X.; Knox, J. E.; Hratchian, H. P.; Cross, J. B.; Adamo, C.; Jaramillo, J.; Gomperts, R.; Stratmann, R. E.; Yazyev, O.; Austin, A. J.; Cammi, R.; Pomelli, C.; Ochterski, J. W.; Ayala, P. Y.; Morokuma, K.; Voth, G. A.; Salvador, P.; Dannenberg, J. J.; Zakrzewski, V. G.; Dapprich, S.; Daniels, A. D.; Strain, M. C.; Farkas, O.; Malick, D. K.; Rabuck, A. D.; Raghavachari, K.; Foresman, J. B.; Ortiz, J. V.; Cui, Q.; Baboul, A. G.; Clifford, S.; Cioslowski, J.; Stefanov, B. B.; Liu, G.; Liashenko, A.; Piskorz, P.; Komaromi, I.; Martin, R. L.; Fox, D. J.; Keith, T.; Al-Laham, M. A.; Peng, C. Y.; Nanayakkara, A.; Challacombe, M.; Gill, P. M. W.; Johnson, B.; Chen, W.; Wong, M. W.; Gonzalez, C.; Pople, J. A. *Gaussian 03*, Revision B.04; Gaussian, Inc.: Pittsburgh PA, 2003.

(15) (a) Becke, A. D. *J. Chem. Phys.* **1993**, *98*, 5648−5652. (b) Lee, C.; Yang, W.; Parr, R. G. *Phys. Rev. B* **1988**, *37*, 785−789.

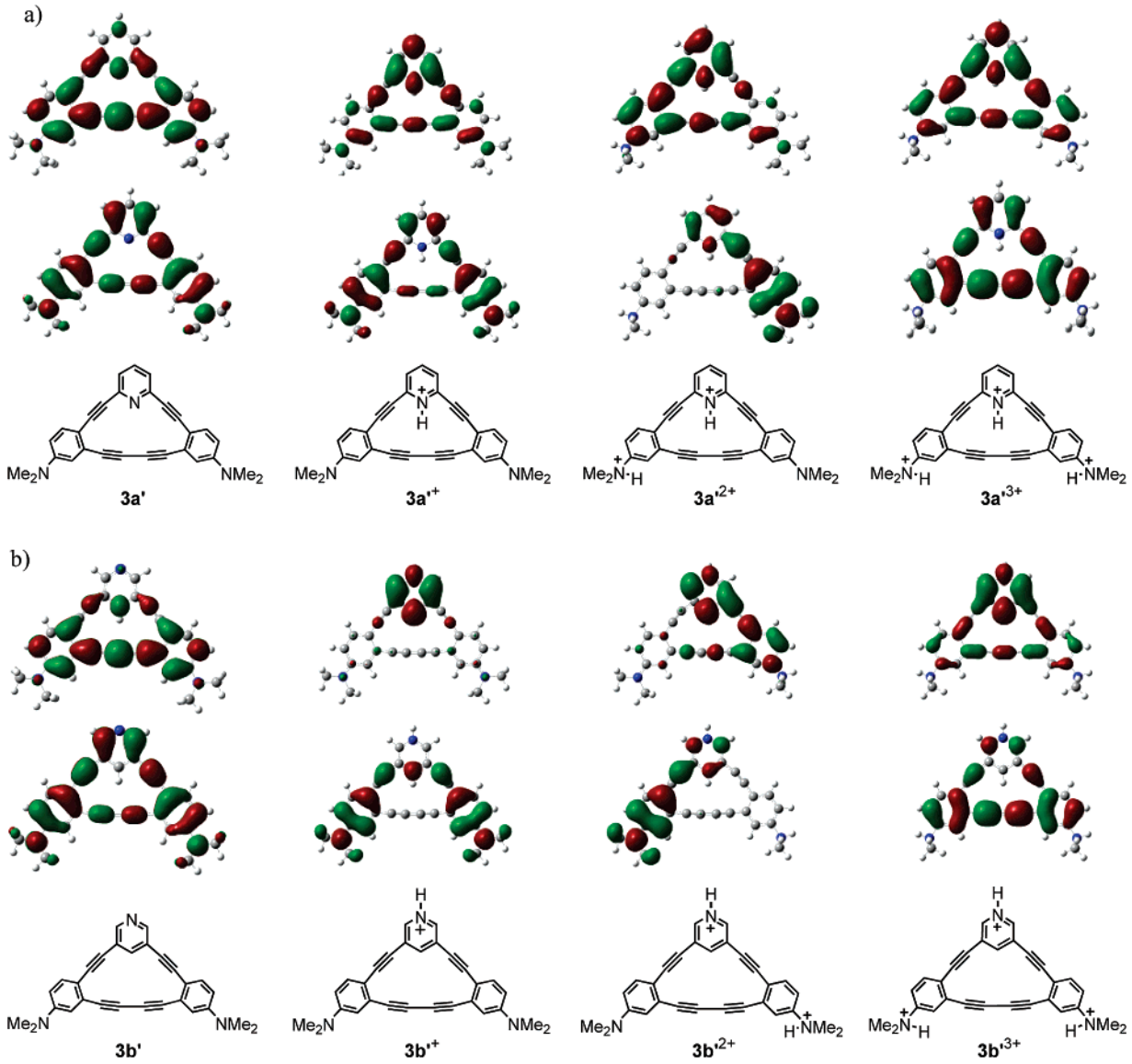

FIGURE 4. Molecular orbital plots (B3LYP/6-31G*) of simplified structures **3a′** (a) and **3b′** (b) of **3a** and **3b**, respectively, in the neutral, monoprotonated, diprotonated, and triprotonated states. The lower plots represent the HOMOs, and the upper plots represent the LUMOs.

to a dark, deep magenta at [TFA] = 10^{-2} M. Further addition of TFA causes a gradual loss of the new bands in the absorption, until at [TFA] = $10^{-0.3}$ M there are no bands past 400 nm. The solution fades from green to very light pink and finally a pale yellow. In the emission spectra, the red band is quenched along with the gradual appearance of a third peak around 540 nm, achieving a pale yellow-green fluorescence.

Titration of **3b** (Figure 6) gave somewhat different results. In the initial stage, the lowest energy band in the absorption spectrum was suppressed and slightly red-shifted to ca. 415 nm at 10^{-2} M TFA, while the fluorescence was significantly quenched at higher than 10^{-4} M, with a red shift of the emission maxima to about 560 nm. The solutions change from pale yellow-green to darker yellow in ambient light, and under UV illumination fade from fluorescent blue-green to a pale yellow-orange at $10^{-2.7}$ M TFA. Additional protonation eliminates any significant absorption past 400 nm, and at 10^{-2} M TFA the emission is suddenly blue-shifted past the neutral compound to ca. 445 nm. The solutions fade to colorless, with the generation of a bright blue fluorescence. The behavior of both compounds is summarized in Table 2. In contrast to our DBPAs, Baxter's pyridannulene systems, which lack donor π-electrons, exhibited only red shifting and quenching with acidification.[5e] Titration of acyclic precursors **6a** and **6b** resulted only in fluorescence quenching with no significant change in λ_{max} (see Figure S3 in the Supporting Information).

We believe the behavior exhibited in **3a** and **3b** arises from predominantly stepwise protonation of the molecules. Because of the π-electron donation from the two NBu_2 groups, it is possible that the pyridine nitrogen is in general protonated first, causing the red shifts in the absorption and emission. Ionization of the acceptor should greatly enhance its electron withdrawal ability, potentially forming a strong charge-transfer system with a low optical band gap. Subsequent protonation of the donor nitrogens then suppresses all charge transfer, leading to a system with only $\pi-\pi^*$ transitions. The donor electrons also allow quick but qualitative evaluation of the magnitude of the effect with use of fluorescence spectroscopy. This easily accessible protonated state could potentially be exploited for advanced nonlinear optical applications. Several of our previously studied

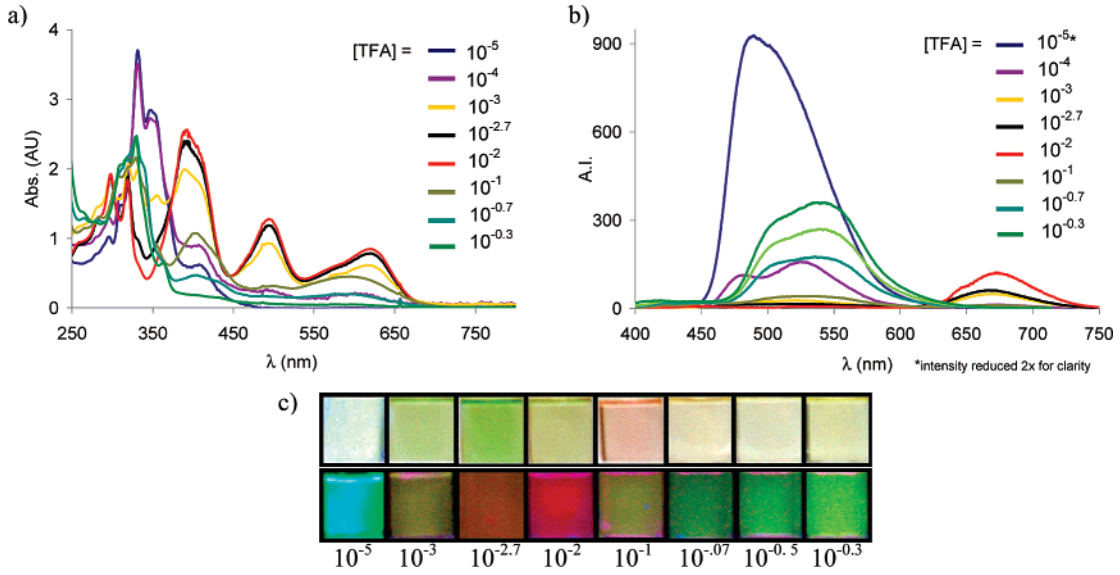

FIGURE 5. (a) Absorption spectra of TFA titration of **3a** in CH_2Cl_2 at ca. 60 μM concentration. (b) Emission spectra of TFA titration of **3a** in CH_2Cl_2. Excitation at 365−385 nm. (c) Solutions of **3a** in CH_2Cl_2 in ambient light against a white background (top) and under illumination by high-intensity 365 nm lamp in the dark (bottom) at indicated [TFA] (M).

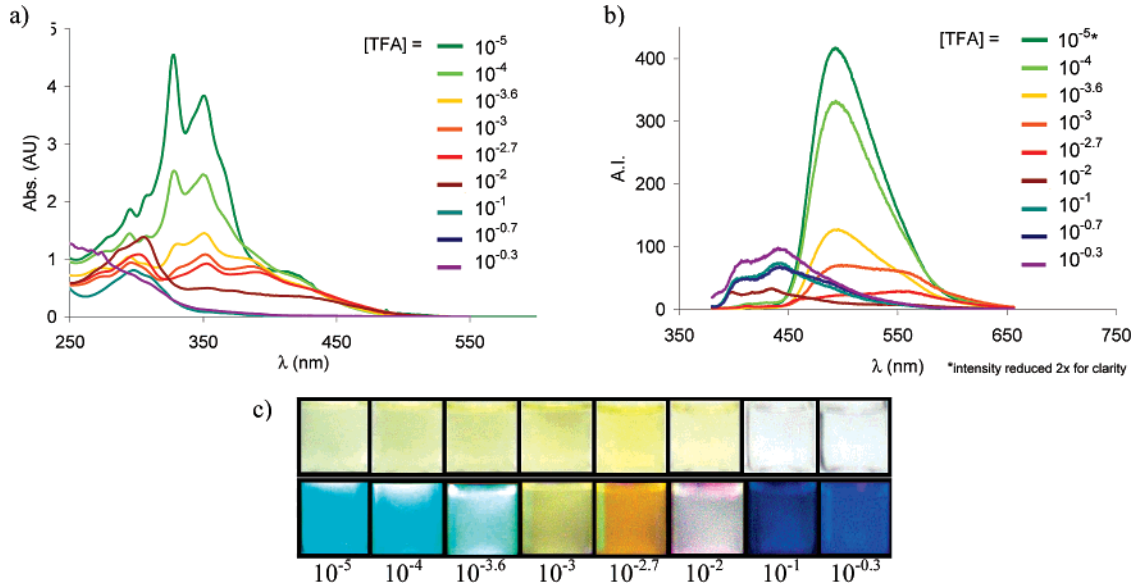

FIGURE 6. (a) Absorption spectra of TFA titration of **3b** in CH_2Cl_2 at ca. 30 μM concentration. (b) Emission spectra of TFA titration of **3b** in CH_2Cl_2. Excitation at 365−400 nm. Interference peaks from excitation wavelength removed for clarity. (c) Solutions of **3b** in CH_2Cl_2 in ambient light against a white background (top) and under illumination by high-intensity 365 nm lamp in the dark (bottom) at indicated [TFA] (M).

TABLE 2. Summary of TFA-Induced Emission Shifting in 3a and 3b in CH_2Cl_2

compd	initial em λ_{max} (nm)	red-shifted em λ_{max} (nm)	$\Delta\lambda_1$ (nm)	blue-shifted em λ_{max} (nm)	$\Delta\lambda_2$ (nm)
3a	490	670[a]	180	541[c]	129
3b	494	560[b]	66	445[c]	115

[a] [TFA] = 10^{-2} M. [b] [TFA] = $10^{-2.7}$ M. [c] [TFA] = $10^{-0.3}$ M.

systems have exhibited significant nonlinear optical susceptibility, with two-photon absorption cross sections that rival literature standards.[7] The greatly narrowed band gap in **3a** at 10^{-2} M TFA may display similar or even better results, particularly since the donor/strong acceptor DBAs[4a] do not display band gaps as small, and acidification of solutions of them causes only blue shifts in both absorption and emission spectra. This effect is not observed to any significant extent in **3b**, likely due to the lack of fully conjugated pathways between the donors and the acceptor. Only a moderate red shift, followed by a dramatic blue shift in the emission is observed. These dynamic emission shifts thus can also serve as a qualitative probe of conjugation efficiency. Although it is not certain whether the red-shifted emission peaks correspond to mono- or diprotonated species (or an equilibrium mixture of both), in both sets of emission spectra the most acidic solutions' emission bands display a weak shoulder somewhat blue-shifted from the maxima. The two emissions may arise from states with either one or both donor nitrogens protonated, but the lack of clearly deconvoluted bands with distinct maxima implies that both are protonated nearly independently or in equilibrium (rather than discretely as in the above FMO calculations). This parallels both our previous work

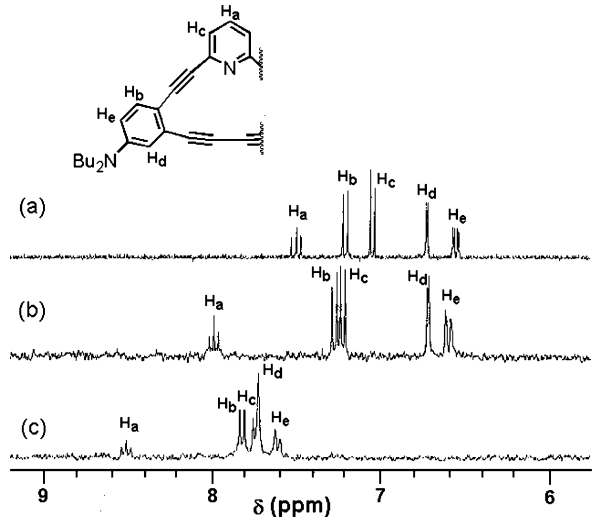

FIGURE 7. ^{1}H NMR spectra in CD_2Cl_2 expanded in the 6−9 ppm region of (a) **3a**, (b) **3a** + 10^{-2} M TFA, and (c) **3a** + $10^{-0.3}$ M TFA (exact H_b/H_c shifts indeterminate due to overlap).

on the acyclic ethynylpyridines as well as Bunz' systems, where only one band for each protonation state was observed.[9a,b] In those cases, the donors are believed to be protonated first, followed by the acceptors. Here, the cumulative donation by two NBu_2 groups to only one pyridine likely accounts for the opposite behavior. The interesting lack of clearly discernible isosbestic points may imply dynamic equilibria during titration rather than distinct species, but the emission wavelengths clearly manifest switching behavior that takes place in predominantly two stages within similar [TFA] ranges for both **3a** and **3b**. Only in the emission spectra of **3a** is there seen a very weak iso-emissive region centered about 630 nm.

To support the hypothesis that the pyridine nitrogen is predominantly protonated first, we prepared samples of **3a** in CD_2Cl_2 and observed the TFA-induced change in proton shifts of the ^{1}H NMR spectra. Figure 7 shows the 6−9 ppm region of solutions of **3a** alone and at 10^{-2} and $10^{-0.3}$ M TFA. Assignment of the protons is based on coupling constants and previous data for **4**,[4a] and is verified by correlation spectroscopy (see the Supporting Information). Comparing the first two spectra clearly reveals significant downfield shifts of the pyridyl protons H_a ($\Delta\delta$ = 0.49) and H_c ($\Delta\delta$ = 0.18) and only slight shifts of the donor segment protons ($\Delta\delta$ = 0.01−0.07), indicative of protonation of the pyridine nitrogen. At $10^{-0.3}$ M TFA, all protons are shifted far downfield. The greater degree of shifting in the donor segment protons ($\Delta\delta$ = 1.00 for both H_d and H_e) in this case indicates protonation at one or both of the dibutylamino nitrogens and generation of an electron-deficient conjugated π-system. A similar but less dramatic stepwise shifting is observed for **3b** (see the Supporting Information). The order of protonation is supported by computations, which indicate that the pyridine-protonated species are 19−31 kcal mol^{-1} lower in energy than the donor-protonated species (Supporting Information, Figures S6 and S7).

Conclusions

We have prepared an isomeric pair of donor-functionalized DBPAs that visibly fluoresce and display weak intramolecular charge transfer behavior. The spectroscopic profiles of the readily obtained molecules illustrate the effect of nitrogen placement in the pyridine acceptor on the degree of conjugation. The unusually large increases in Stokes shifts upon cyclization are believed to result from the combination of donor π-electrons, LUMO localization on the diacetylene bridge formed in the last synthetic step, and the cross-conjugated "kink" in the 15-membered macocycles. It has been demonstrated that fluorescence spectroscopy can be used to probe the behavior of a donor/acceptor fluorophore that can be protonated at both donor and acceptor sites. In particular, the absorption and emission spectra for **3a** at moderate (10^{-2} M) acid concentration suggest a monoprotonated state with a particularly narrow optical band gap, prompting the question of its candidacy as a component in nonlinear optical devices. The dynamic emission switching bears striking resemblance to previous studies by us and others involving independent manipulation of frontier molecular orbitals, leading to potential applications as fluorescent ion sensors.[9a,b,16] To our knowledge, this is the first reported instance of such behavior in conjugated acetylenic macrocycles. The calculated overlapping FMOs in neutral **3a** and **3b** further imply that independent manipulation of HOMOs and LUMOs may not require as dramatic of a spatial separation as previously assumed.

Experimental Section

General Methods. These have been described previously.[4a]

Precursor 6a. A mixture of 2,6-dibromopyridine (**5a**, 52 mg, 0.22 mmol), donor diyne **4**[4a] (317 mg, 0.66 mmol), KOH (123 mg, 2.20 mmol), THF (20 mL), *i*-Pr_2NH (20 mL), and MeOH (1 mL) was bubbled with Ar with stirring for 30 min. $Pd(PPh_3)_4$ (15 mg, 0.013 mmol) and CuI (5 mg, 0.026 mmol) were quickly added and the mixture was bubbled for an additional 20 min. The temperature was raised to 55 °C and the reaction stirred until complete by TLC (ca. 18 h). The mixture was evaporated and the residue chromatographed on silica gel (2:1 hexanes:CH_2Cl_2) to yield **6a** (164 mg, 84%) as a yellow oil. ^{1}H NMR (300 MHz, $CDCl_3$) δ 7.53 (t, J = 7.2 Hz, 1H), 7.42 (d, J = 9.0 Hz, 2H), 7.34 (d, J = 7.8 Hz, 2H), 6.72 (d, J = 2.4 Hz, 2H), 6.54 (dd, J = 7.8, 2.4 Hz, 2H), 3.27 (t, J = 7.5 Hz, 8H), 1.56 (quin, J = 7.2 Hz, 8H), 1.35 (sext, J = 7.2 Hz, 8H), 1.15 (s, 42H), 0.96 (t, J = 7.2 Hz, 12H). ^{13}C NMR (75 MHz, $CDCl_3$) δ 148.1, 144.7, 135.7, 134.2, 127.4, 125.5, 115.4, 111.9, 110.8, 106.7, 93.5, 90.2, 90.2, 50.8, 29.5, 20.5, 19.0, 14.2, 11.7. IR (NaCl) ν 2955, 2937, 2858, 2202, 2147, 1655, 1639, 1594, 1572, 1552, 1534, 1509, 1465, 1438, 1397, 1367 cm^{-1}. MS (APCI) *m/z* ([isotope], %) 894.6 ([M^+], 100), 895.6 ([M^{+13}C], 78), 896.6 ([$M^{+2\,13}$C], 35). UV (CH_2Cl_2) λ_{max} (log ϵ) 346 (4.55), 390 (4.70). Em λ_{max} 427.

Precursor 6b. A mixture of 3,5-dibromopyridine (**5b**, 47 mg, 0.20 mmol), donor diyne **4**[4a] (240 mg, 0.50 mmol), KOH (94 mg, 1.67 mmol), THF (20 mL), *i*-Pr_2NH (20 mL), and MeOH (1 mL) was bubbled with Ar with stirring for 30 min. $Pd(PPh_3)_4$ (14 mg, 0.012 mmol) and CuI (4.6 mg, 0.024 mmol) were quickly added and the mixture was bubbled for an additional 20 min. The temperature was raised to 55 °C and the reaction stirred until complete by TLC (ca. 18 h). The mixture was evaporated and the residue chromatographed on silica gel (2:1 hexanes:CH_2Cl_2) to yield **6b** (97 mg, 54%) as a yellow oil. ^{1}H NMR (300 MHz, $CDCl_3$) δ 8.55 (d, J = 2.1 Hz, 2H), 7.84 (t, J = 2.1 Hz, 1H), 7.32 (d, J = 9.0 Hz, 2H), 6.73 (d, J = 2.8 Hz, 2H), 6.55 (dd, J = 9.0, 2.8 Hz, 2H), 3.28 (t, J = 7.8 Hz, 8H), 1.57 (quin, J = 7.5 Hz, 8H), 1.38 (sext, J = 7.8 Hz, 8H), 1.17 (s, 42H), 0.96 (t, J = 7.2 Hz, 12H). ^{13}C NMR (75 MHz, $CDCl_3$) δ 150.0, 148.0, 140.5, 136.6, 127.1, 121.1, 115.5, 111.9, 110.9, 106.5, 93.8, 93.5, 86.7, 50.8, 29.5, 20.5, 19.0, 14.2, 11.6. IR (NaCl) ν 2952, 2938, 2859, 2208, 2151, 1718, 1593,

(16) Huang, J.-H.; Wen, W.-H.; Sun, Y.-Y.; Chou, P.-T.; Fang, J.-M. *J. Org. Chem.* **2005**, *70*, 5827−5832.

1568, 1536, 1503, 1464, 1432, 1396, 1371 cm^{-1}. MS (APCI) *m*/*z* ([isotope], %) 894.6 ([M^+], 100), 895.6 ([$M^{+13}C$], 70), 896.6 ([$M^+2^{13}C$], 33). UV (CH_2Cl_2) λ_{max} (log ϵ) 348 (4.65), 383 (4.72). Em λ_{max} 421.

Annulene 3a. Precursor **6a** (120 mg, 0.13 mmol) was dissolved in THF (20 mL), Et_2O (20 mL), and MeOH (10 mL). TBAF (5.4 mL, 5.4 mmol, 1 M in THF) was added and the mixture was stirred for ca. 18 h. The mixture was concentrated in vacuo, rediluted in Et_2O, and washed with H_2O (2×). The organic phase was dried ($MgSO_4$) and concentrated in vacuo to give an amber oil. The deprotected material was dissolved in pyridine (50 mL) and injected into a mixture of $Cu(OAc)_2$ (669 mg, 3.4 mmol) and CuCl (265 mg, 2.7 mmol) in pyridine (340 mL) and MeOH (50 mL) over 40 h with stirring at 65 °C. After injection was complete, the solution was stirred for an additional 24 h, then evaporated to a blue-green oil. The residue was redissolved in Et_2O and washed with H_2O (3×). The organic phase was dried ($MgSO_4$), concentrated in vacuo, and filtered through a pad of silica (1:1 hexanes:CH_2Cl_2)to yield **3a** (66 mg, 85%) as a bright yellow solid. Mp 131−133 °C. ^1H NMR ($CDCl_3$) δ 7.49 (t, J = 7.8 Hz, 1H), 7.23 (d, J = 8.7 Hz, 2H), 7.07 (d, J = 7.8 Hz, 2H), 6.72 (d, J = 2.7 Hz, 2H), 6.51 (dd, J = 8.7, 2.7 Hz, 2H), 3.25 (t, J = 7.8 Hz, 8H), 1.54 (quin, J = 7.8 Hz, 8H), 1.34 (sext, J = 7.8 Hz, 8H), 0.96 (t, J = 7.2 Hz, 12H). ^{13}C NMR ($CDCl_3$) δ 148.2, 145.4, 136.9, 131.7, 129.0, 121.2, 115.0, 112.3, 112.1, 94.1, 92.2, 82.3, 78.3, 51.0, 29.5, 20.5, 14.2. IR (NaCl) ν 2951, 2924, 2866, 2193, 1682, 1652, 1591, 1570, 1533, 1502, 1451, 1366 cm^{-1}. MS (APCI) *m*/*z* ([isotope], %) 580.4 ([M^+], 100), 581.4 ([$M^{+13}C$], 44), 582.4 ([$M^+2^{13}C$], 8). UV (CH_2Cl_2) λ_{max} (log ϵ) 347 (4.90), 407 (4.24). Em λ_{max} 490.

Annulene 3b. Precursor **6b** (90 mg, 0.10 mmol) was dissolved in THF (20 mL), Et_2O (20 mL), and MeOH (10 mL). TBAF (6.0 mL, 6.0 mmol, 1 M in THF) was added and the mixture was stirred for ca. 18 h. The mixture was concentrated in vacuo, rediluted in Et_2O, and washed with H_2O (2×). The organic phase was dried ($MgSO_4$) and concentrated in vacuo to give an amber oil. The deprotected material was dissolved in pyridine (37 mL) and injected into a mixture of $Cu(OAc)_2$ (499 mg, 2.5 mmol) and CuCl (198 mg, 2.0 mmol) in pyridine (254 mL) and MeOH (37 mL) over 40 h with stirring at 65 °C. After injection was complete, the solution was stirred for an additional 24 h, then evaporated to a blue-green oil. The residue was redissolved in Et_2O and washed in H_2O (3×). The organic phase was dried ($MgSO_4$), concentrated in vacuo, and filtered through a pad of silica (1:1 hexanes:CH_2Cl_2) to yield **3b** (25 mg, 77%) as a yellow solid. Mp 181−183 °C. ^1H NMR ($CDCl_3$) δ 8.75 (t, J = 1.5 Hz, 1H), 8.39 (d, J = 1.5 Hz, 2H), 7.24 (d, J = 9.0 Hz, 2H), 6.77 (d, J = 2.4 Hz, 2H), 6.58 (dd, J = 9.0, 2.4 Hz, 2H), 3.27 (t, J = 8.1 Hz, 8H), 1.56 (quin, J = 8.1 Hz, 8H), 1.32 (sext, J = 7.5 Hz, 8H), 0.97 (t, J = 7.5 Hz, 12H). ^{13}C NMR ($CDCl_3$) δ 150.5, 148.1, 145.4, 131.2, 127.7, 122.0, 115.3, 112.5, 112.2, 100.2, 98.1, 90.6, 83.2, 51.0, 29.5, 20.5, 14.3. IR (NaCl) ν 2951, 2925, 2866, 2218, 2191, 1771, 1739, 1696, 1684, 1650, 1594, 1567, 1557, 1538, 1504, 1455,1399, 1365 cm^{-1}. MS (APCI) *m*/*z* ([isotope], %) 580.4 ([M^+], 100), 581.4 ([$M^{+13}C$], 37), 582.3 ([$M^+2^{13}C$], 11). UV (CH_2Cl_2) λ_{max} (log ϵ) 352 (4.70), 408 (4.09). Em λ_{max} 494.

TFA Titration of 3a and 3b. Solutions of **3a** and **3b** were prepared in spectrophotometric grade CH_2Cl_2 (ca. 1 mg in 360 μL, UV cutoff 204 nm) and portioned equally into nine 1-dram glass screw cap vials. Trifluoroacetic acid was diluted to the indicated concentrations ranging from 10^{-5} to $10^{-0.3}$ M in 10 mL portions of CH_2Cl_2. Aliquots (2 mL) of the TFA solutions were added to each solution of analyte. The solutions were capped, shaken, and pipetted into a four-sided quartz spectrophotometry cuvette, and the UV−vis and fluorescence spectra were then taken immediately. Photographs were taken within 1 h of preparation of each sample.

Acknowledgment. We thank the National Science Foundation (CHE-0414175 and -0718242) for financial support and Dr. Lev N. Zakharov for crystallographic data. E.L.S. and S.P.M. acknowledge the NSF for IGERT fellowships (DGE-0549503).

Supporting Information Available: Copies of ^1H NMR spectra for **3a**,**b** and **6a**,**b**; crystallographic data for **3a**,**b**; computational details; emission spectra of **3a** titrated with TFA in MeOH; and emission spectra of **6a** and **6b** titrated with TFA in CH_2Cl_2. This material is available free of charge via the Internet at http://pubs.acs.org.

JO070827C